Computers & Geosciences 62 (2014) 71–79

Contents lists available at ScienceDirect

Computers & Geosciences

journal homepage: www.elsevier.com/locate/cageo

A continuative variable resolution digital elevation model for ground-based photogrammetry

Zhaoqin Liu [a,b], Man Peng [a], Kaichang Di [a,*]

[a] State Key Laboratory of Remote Sensing Science, Institute of Remote Sensing and Digital Earth, Chinese Academy of Sciences, Beijing, PR China
[b] Science and Technology on Aerospace Flight Dynamics Laboratory, Beijing, PR China

ARTICLE INFO

Article history:
Received 8 March 2013
Received in revised form
10 September 2013
Accepted 3 October 2013
Available online 11 October 2013

Keywords:
Digital elevation model
Continuative variable resolution
Polar coordinates
Ground-based photogrammetry
Terrestrial laser scanning

ABSTRACT

A new digital elevation model (DEM) is presented for accurate surface representation in photogrammetric processing of stereo ground-based imagery. This model is named the continuative variable resolution DEM (cvrDEM). In contrast to traditional grid-based DEMs that have only one fixed resolution, this new model can provide resolutions that vary depending on the range represented in the ground-based imagery. Functions for deriving radial and angular resolutions from the cvrDEM have been derived, and a corresponding storage structure for the polar coordinates has been developed. Experimental results using publically available NASA Mars Exploration Rover 2003 imagery demonstrate the effectiveness of the cvrDEM model: It can significantly reduce storage space while fully maintaining the most useful level of mapping accuracy relevant to the range from the imaging station. A terrestrial laser scanning data set was also used to validate the effectiveness of the cvrDEM.

1. Introduction

While aerial photogrammetry has been the major approach for large-scale topographic mapping, ground-based close-range photogrammetry is also widely used in topographic mapping (Slama et al., 1980; Wang, 1990). A recent highlighted application of ground-based photogrammetry to topographic mapping has been developed for the NASA Mars Exploration Rover 2003 (MER) mission, where the Spirit and Opportunity rovers have acquired a vast amount of stereo images using the onboard navigation (Navcam), panoramic (Pancam) and hazard avoidance (Hazcam) cameras. These ground images have been extensively used to generate Digital Elevation Models (DEMs), orthoimages and rover localization data to support mission operations (e.g., traverse planning) and various scientific investigations (Li et al., 2005; Alexander et al., 2006; Di et al., 2008). In the new Mars rover mission, the NASA Mars Science Laboratory, topographic products are being generated from stereo images acquired by the Curiosity rover for similar uses. In addition to stereo photogrammetry, ground-based LiDAR (Light Detection And Ranging) is another highly efficient approach to rapid acquisition of 3D terrain and surface data with a high level of accuracy (Maune, 2007; Oliveira et al., 2012). While the density and accuracy of 3D points obtained from aerial photogrammetry or air-borne laser scanning are generally homogeneous within one project area, the density and accuracy of 3D points obtained from ground-based photogrammetry or terrestrial laser scanning are highly inhomogeneous and, usually, they decreases with the increase of the range (distance from the survey station to the mapping target). Di and Li (2007) presented a comprehensive analysis of the topographic mapping capabilities of the stereo images of the MER rovers. Ideally, the representation of the mass 3D points generated from ground-based imagery should maintain the level of accuracy over different ranges and also save storage space.

To date, grid-based DEMs, Triangulated Irregular Network (TIN)-based DEMs, and digital contours (Contour-based DEMs) have all been widely used for digital terrain representation (Moore et al., 2006; Li et al., 2004; Maune, 2007). Among these data structures, the grid-based DEM has been the most commonly used due to its advantages of simplicity and relatively compact storage requirements (Li et al., 2004). On the other hand, there are disadvantages to the grid-based DEM: it cannot handle abrupt changes in elevation and the size of the grid mesh directly affects both the obtained resolution of terrain representation and computational efficiency. The grid-based DEM cannot accommodate various grid sizes to reflect areas of different accuracies from the mass 3D data generated from ground-based photogrammetry. As the entire area adopts only a single level of resolution, it may cause either storage space redundancy from a grid size that is smaller than necessary over most parts of the area, or a loss of accuracy needed in certain areas if a large grid size is chosen.

TIN-based DEMs offer a relatively easy way of incorporating variability into the DEM. The density of the TIN triangles can be

* Corresponding author. Tel.: +86 106 486 8229.
E-mail address: kcdi@irsa.ac.cn (K. Di).

0098-3004/$ - see front matter © 2013 Elsevier Ltd. All rights reserved.
http://dx.doi.org/10.1016/j.cageo.2013.10.001

varied to reflect the roughness of the terrain. Also, it increases data storage efficiency as it stores only the nodes and lines of the triangles along with topology indexes. However, since the triangles are irregular, a TIN is usually not as easy to manipulate as a grid-based DEM. And when the elevations of the positions within the triangles are needed, interpolations are usually necessary.

In computer graphics field, interactive visualization of very large-scale terrain data imposes several efficiency problems. To reduce rendering complexity without affecting the visual accuracy, the terrain model must provide mechanism to quickly extract surface representations at variable precisions (Zhang et al., 2005; Zhao et al., 2006). To this end, multi-resolution models have been developed that adapt to the complexity of the rendered model. Bertolotto et al. (1994) defined a hierarchical model for representing hypersurfaces in any dimension. De Floriani et al. (1996) provided a critical survey of multi-resolution terrain models and analyzed their time efficiencies and complexities. Mahdi et al. (1998) compared existing hierarchical triangulation techniques, several parameters were introduced to measure how esthetically appealing a hierarchical terrain representation is. Fredrik and Jungert (2000) developed a grid-based terrain data model with irregular data points, which includes quantitative characteristic for visualization and a qualitative representation for feature analysis. Evans et al. (2001) presented a restricted form of a triangulated irregular network (RTIN) and demonstrated its storage efficiency. Pajarola (2002) reviewed several quadtree based triangulation methods and compared their strengths and weaknesses with respect to efficiency. Pajarola and Gobbetti (2007) analyzed and compared multi-resolution models based on tiled blocks, nested regular grids, and quadtree or triangle bintree triangulations for interactive terrain rendering application. Suárez and Plaza (2009) followed the RTIN scheme and presented two algorithms for adaptive refining/coarsening RTIN terrain meshes. Xie et al. (2013) proposed a hybrid data structure for seamless integration of TINs and Grids in order for multi-resolution surface representation. Zarrabeitia and Mederos (2013) proposed an algorithm to obtain a multiresolution representation of a terrain based on level-curve information; it removes iteratively the less important level curves to facilitate visualization of the terrain. These multi-resolution models are used for interactive terrain visualization, and they don't take into consideration mapping accuracy. If and how mapping accuracy can be considered in these multi-resolution models is an interesting topic for future research.

In ground-based photogrammetry, finding digital elevation models that combine high accuracy with low data storage requirements is very challenging. To reduce data storage space while maintaining mapping accuracy across different ranges, we have developed the continuative variable resolution DEM (cvrDEM) model for the representation of 3D surfaces generated by ground-based photogrammetry. Being difference from grid-based DEM with uniform resolution in Cartesian coordinate system, cvrDEM model is composed of sampling points with variable resolution based on polar coordinates. The sampling parameters of the polar coordinates are determined in such a way that the mapping accuracy of the point is maintained.

In the human visual system, the cortical mapping is performed through a space-variant sampling strategy, with the sampling period increasing almost linearly with the distance from the fovea. In mimicking this mechanism, the log-polar mapping, which has properties of rotation and sacling invariance, has been developed in image processing and computer vision field. Wolberg and Zokai (2000) introduced a log-polar registration module to accommodate arbitrary rotation angels and a wide range of scale changes, and a hierarchical image registration algorithm was developed for affine motion recovery. Traver and Bernardino (2010) presented a review of log-polar imaging for robotic vision applications such as visual attention, target tracking, egomotion estimation, and 3D perception; all these applications benefited from the high resolution of the fovea region. Based on log-polar coordinate system, Masuda (2009) proposed a method for coarse registration of multiple range images using a log-polar height map as the key for establishing correspondence. On the contrary to the log-polar image representation with higher resolution at the fovea and reduced resolution at the periphery, Onkarappa and Sappa (2013) proposed a novel and simple space-variant image representation with higher resolution at the periphery and lower resolution at the fovea and it was proved to be a better representation in navigational applications. Overall, log-polar and polar image sampling methods have been successfully applied in computer vision applications. Now, polar and log-polar projection tools (e.g., MATLAB tools) are openly available for image conversion between Cartesian coordinates to polar/log-polar coordinates. These tools are not directly applicable to terrain data of mass points; mapping accuracies cannot be handled either. So far, polar or log-polar sampling scheme has not been investigated in terrain modeling for space variant representation. For terrain mapping and modeling, it is essential to maintain the mapping accuracy of the original mass points. Based on theoretical mapping accuracy analysis and the polar sampling scheme, the proposed cvrDEM provides a new solution of terrain modeling that maintains mapping accuracies of massive points with different ranges and avoids over-sampling and under-sampling. This is particularly useful and important for point cloud data generated from ground-based photogrammetry and terrestrial laser scanning.

The concepts and processes of cvrDEM construction are presented in Section 2. Experimental results based Mars rover imagery and terrestrial laser scanning data are presented in Section 3. Conclusions and ideas for future research are given in Section 4.

2. The cvrDEM model

2.1. Conceptual basis of cvrDEM

In grid-based DEMs, sampling points are distributed evenly. This condition is unable to represent differences in accuracy caused by varying ranges in photogrammetric processing of ground-based imagery. As a result, the grid-based DEM may be over-sampled for distant ranges (wasting storage space) while under-sampled for closer ranges (losing accuracy). To overcome this problem, cvrDEM has been designed to sample the terrain using different resolutions for different ranges according to the varying useful level of mapping accuracy, so that the DEM can represent the terrain as accurately as possible while occupy as small a data storage space as possible. As shown in Fig. 1, the resolution of cvrDEM continually changes along the range, while the direction is sampled at even interval, so that the final sampling points are arranged regularly on the concentric circles. In the center of the DEM, there may be a hole because that area is covered by the imaging station itself. Unlike the grid-based DEM, it is easy to use polar coordinates to represent these sampling points.

There are two apparent advantages to cvrDEM: (1) it can maintain the attainable accuracies at all ranges with variable resolutions while reducing data storage space, and (2) these variable-resolution sampling points can be efficiently represented and managed using a polar coordinate system.

2.2. Method for cvrDEM construction

The construction of a cvrDEM is based on the 3D points derived from stereo images and theoretical accuracy analysis of the cvrDEM parameters using close-range photogrammetry principles. A diagram of the overall approach is shown in Fig. 2. A polar

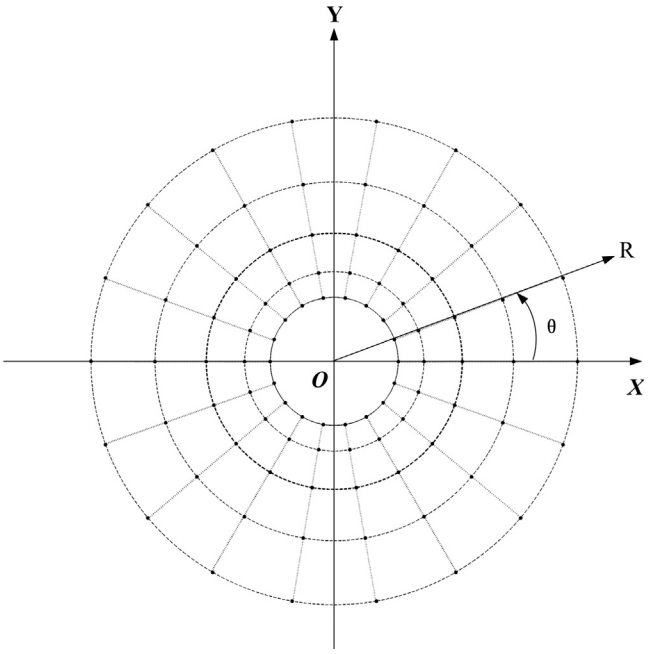

Fig. 1. Conceptual illustration of cvrDEM coverage and the coordinate systems.

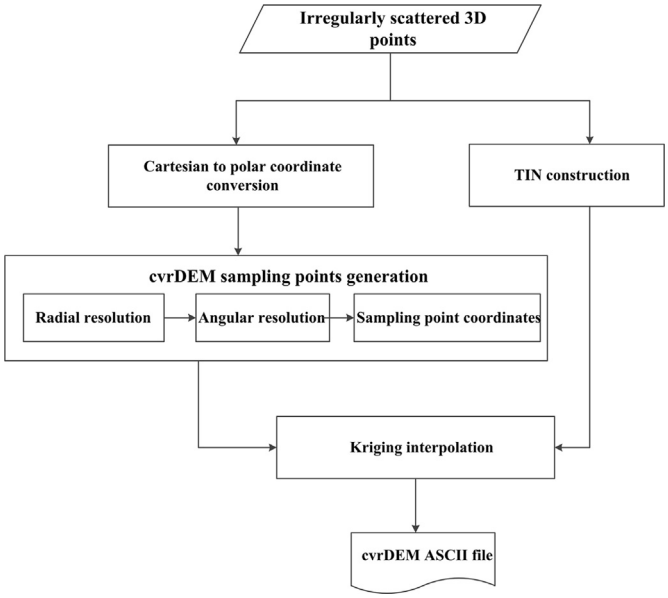

Fig. 2. Diagram of cvrDEM construction.

coordinate system and a Cartesian coordinate system are defined. For both, the site center is the origin. Conversion from Cartesian coordinates to polar coordinates is straightforward. As the data source, 3D coordinates of matched feature points are generated in the Cartesian coordinate system. Usually these are irregularly distributed. In order to calculate the coordinates of the sampling points in cvrDEM, it is important to determine radial and angular resolutions based on theoretical accuracy analysis. Then, the polar coordinates of all the required sampling points are converted from the polar coordinate system to Cartesian coordinates. Finally, 3D coordinates of the sampling points are generated by Kriging interpolation from the TIN and are stored in the cvrDEM database structure. Key algorithms of the method are given below in more detail.

2.2.1. Polar coordinates

As shown in Fig. 1, first the local Cartesian coordinate system, which we call Site Frame XOY, is defined as follows: the site center (imaging station center) is set to be the origin, the *X*-axis of the site frame points to local east, the *Z*-axis points up in the local normal direction, and the *Y*-axis is defined to form a right-handed system.

Then, the polar coordinate system is built based on the Site Frame. The origin is the same as that of the Cartesian system. The polar axis (zero angle direction) is the same as the positive *X*-axis, and the angle increases counter-clockwise from 0° to 360°. The radial coordinate, or radius, is represented as the distance from the origin. The conversion from Cartesian coordinate to polar coordinate is straightforward and simple, thus the equations are omitted here.

2.2.2. Determination of radial and angular resolution parameters

Determination of the appropriate resolution of an interpolated DEM is a compromise between achieving fidelity to the true surface and considering practical limits related to the density and accuracy of the source data (Wilson and Gallant, 2000). For cvrDEM, radial resolution and angular resolution are the two key factors: They should be determined according to the camera parameters so as to maintain the attainable accuracies.

To simplify the derivation, as shown in Fig. 3, we assume that the stereo pair was acquired in a "normal case" configuration, i.e., where the two camera axes are parallel to each other and perpendicular to the baseline (Di and Li, 2007). We also assume that the two cameras are identical and have no lens distortions. For such a configuration, the elevation of the object point can be calculated using the following parallax equation:

$$Z_p = \frac{B}{p} y = \frac{Y_p}{f} y \tag{1}$$

where f is the focal length of the cameras, B is the length of the stereo baseline, and p is the stereo parallax of the corresponding points which is calculated as $p = x - x'$. Through error propagation, the elevation accuracy (standard error) is represented as (Di and Li, 2007)

$$\sigma_Z = \sqrt{\left(\frac{Y_p^2}{Bf}\right)^2 \left(\frac{y}{f}\right)^2 \sigma_p^2 + \left(\frac{Y_p}{f}\right)^2 \sigma_y^2} \tag{2}$$

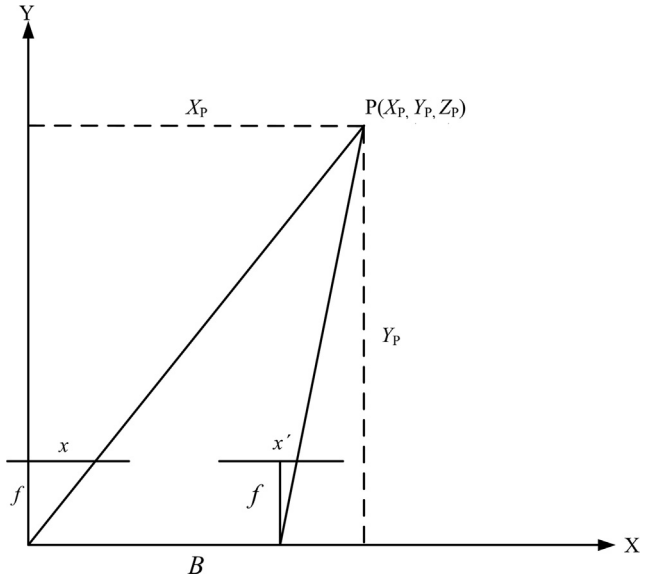

Fig. 3. "Normal case" stereo configuration of ground images (Di and Li, 2007).

where f and B are the same as defined in Eq. (1), σ_p is the parallax measurement error, and σ_y is the image measurement error in y (row) directions in the image space. From Eq. (2), we can easily understand that the measurement error decreases when the focal length and/or the baseline length increase. Meanwhile, the elevation error (σ_z) is dependent not only on the range (Y_p), but also on the position of the object in the image. At a given range, the minimum error of Z lies on the horizontal line passing through the image center (where $y=0$), and the maximum errors of Z lie on the top and bottom margins of the image. Thus the minimum error of elevation can be represented as

$$\sigma_Z = \frac{Y_P}{f}\sigma_y = \frac{r}{f}\sigma_y = \frac{\sigma_y}{f}r = kr \tag{3}$$

where r is range of the ground point in a polar coordinate system and equals to Y_p.

Using the MER Navcam camera parameters (Table 1) and setting σ_y to be one pixel, we can calculate the maximum and minimum errors of the MER Navcam at different distances from the site center. These are illustrated in Fig. 4. From Eq. (3) and Fig. 4, it easily can be seen that the minimum elevation error is proportional to the distance from the target to the site center.

In fact, when σ_y is set to be one pixel, the minimum elevation error kr equals to the ground resolution of one pixel at the range r. If we set the radial resolution at range r to be kr, all the ground points (even if they are pixel-by-pixel dense 3D points) generated from stereo images will be kept; this ensures that the mapping accuracies of the ground points are fully maintained. As a rule of thumb in aerial stereo-photogrammetry, a DEM with a resolution of 3–5 pixels are usually sufficient to maintain the mapping capability of the stereo images. Therefore, the radial resolution of cvrDEM at range r is set to be proportional to kr with a coefficient n ($1 \le n \le 5$), i.e., $\Delta_r = n \times kr = \lambda r$. The coefficient λ is then used as the radial resolution parameter for the cvrDEM and calculated as

$$\lambda = n \times k = n \times (pixel\_size/f) \tag{4}$$

The angular resolution is determined directly by the IFOV (Instantaneous Field Of View) of the camera. It is represented as

$$\delta_\theta = m \times \arctan(pixel\_size/f) \tag{5}$$

where m is a coefficient that is greater than or equal to 1. For the MER Navcam, the IFOV value is 0.0469° (0.0008 rad). The default value of m is 1 to allow pixel-by-pixel dense 3D points.

Similar to point cloud data generated from ground-based photogrammetry, terrestrial laser scanning data are inhomogeneous: the closer to the scanning center, the denser the point cloud data. To build a cvrDEM for a terrestrial laser scanning data of one site, δ_θ can be determined by the angular resolution of the laser scanner, λ is determined by the ground spacing of the laser points on the ground at range r.

2.2.3. Sampling point coordinates in cvrDEM

Once the radial and angular resolution parameters have been determined, the coordinates of the sampling points can be calculated through the following steps. For ease in storing the polar coordinates of cvrDEM in a matrix form, we set the angular coordinates as rows and the radial coordinates as columns.

If the stereo images cover a full panorama, directly set the maximum angle as $\theta_{max}=360°$ and the minimum angle as $\theta_{min}=0°$. Otherwise, sort the angles of the matched dense points to the site center point with reference to zero direction and find the maximum and minimum angles θ_{max} and θ_{min}. Then, the sampling point angle can be calculated from the following equation:

$$\theta_i = \theta_{min} + (i-1)\,\delta_\theta \tag{6}$$

where i is the serial number. Thus, the total number of rows N_θ of the cvrDEM is calculated as

$$N_\theta = INT((\theta_{max} - \theta_{min})/\delta_\theta) + 1 \tag{7}$$

where *INT* stands for rounding operation.

Radial coordinates should be sampled with continuative variable resolutions along the distance direction. Suppose the radial coordinate of the first sampling point is $r_1 = r_{min}$, then the radial resolution of the cvrDEM at r_{min} is

$$\Delta_1 = \lambda r_1 = \lambda r_{min} \tag{8}$$

and the radial coordinate of the second sampling point r_2 can be calculated as

$$r_2 = r_1 + \Delta_1 = r_{min} + \lambda r_{min} = r_{min}(1+\lambda). \tag{9}$$

Consequently, the next radial coordinate of the sampling point r_3 can be calculated as

$$r_3 = r_2 + \Delta_2 = r_2 + \lambda r_2 = r_2(1+\lambda) = r_{min}(1+\lambda)^2. \tag{10}$$

Table 1
Camera parameters of MER Navcam (Maki et al., 2003).

Stereo base	20 cm
Focal length	14.67 mm
Image dimension	1024 × 1024 pixels
Pixel size	12 μm
Field of view	45 × 45°

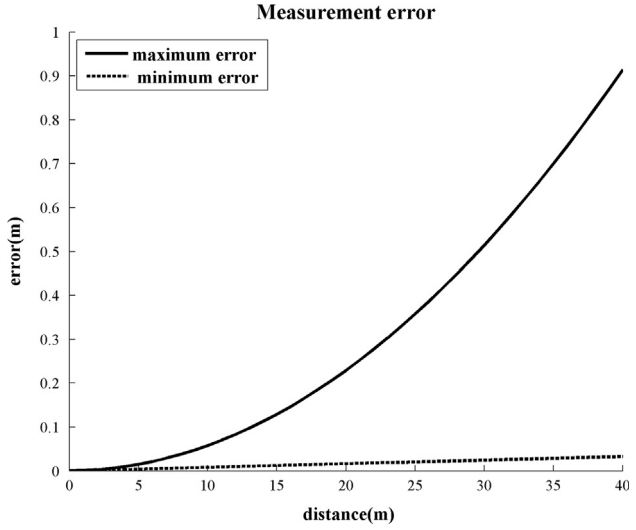

Fig. 4. Measurement errors of elevation vs. distance.

Table 2
cvrDEM data structure.

X_O	Y_O			
θ_{min}	N_θ			
r_{min}	N_r			
λ	δ_θ			
nodata_value				
Z_{θ_1,r_1}	Z_{θ_1,r_2}	⋯	Z_{θ_1,r_j}	⋯ $Z_{\theta_1,r_{N_r}}$
Z_{θ_2,r_1}	Z_{θ_2,r_2}	⋯	Z_{θ_2,r_j}	⋯ $Z_{\theta_2,r_{N_r}}$
⋯	⋯	⋯	⋯	⋯ ⋯
Z_{θ_i,r_1}	Z_{θ_i,r_2}	⋯	Z_{θ_i,r_j}	⋯ $Z_{\theta_i,r_{N_r}}$
⋯	⋯	⋯	⋯	⋯ ⋯
$Z_{\theta_{N_\theta},r_1}$	$Z_{\theta_{N_\theta},r_2}$	⋯	$Z_{\theta_{N_\theta},r_j}$	⋯ $Z_{\theta_{N_\theta},r_{N_r}}$

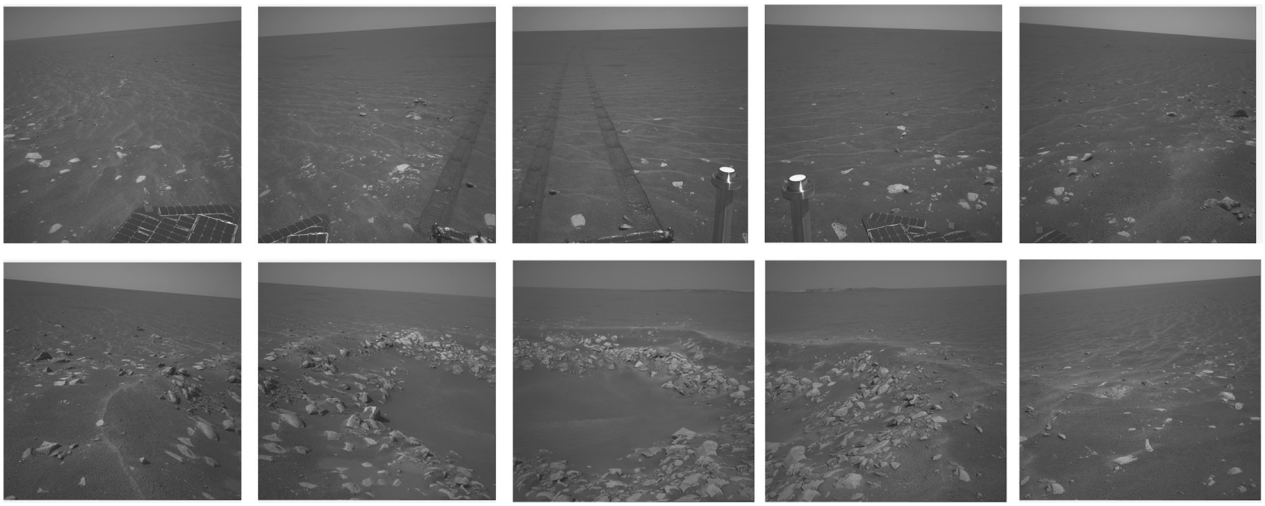

Fig. 5. Left images of a 360° panorama acquired by the Opportunity rover Navcam at position 6444 on Sol 85.

In general form, we have

$$r_j = r_{min}(1+\lambda)^{j-1} \tag{11}$$

Therefore, the number of columns N_r of the cvrDEM is

$$N_r = INT(\log_{(1+\lambda)}(r_{max}/r_{min}))+1 = INT(\ln(r_{max}/r_{min})/\ln(1+\lambda))+1 \tag{12}$$

After the numbers of rows and columns of the cvrDEM are determined, we can calculate the Cartesian coordinates of the sampling points as

$$\begin{cases} X_{(i,j)} = r_{min}(1+\lambda)^{j-1}\cos(\theta_{min}+(i-1)\,\delta_\theta) & i=1,2,\cdots N_\theta \\ Y_{(i,j)} = r_{min}(1+\lambda)^{j-1}\sin(\theta_{min}+(i-1)\,\delta_\theta) & j=1,2,\cdots N_r \end{cases} \tag{13}$$

while $(X_{i,j}, Y_{i,j})$ are the Cartesian coordinates of the point (θ_i, r_j).

As a result, the distance between the neighboring sampling points are non-uniform in radial direction: the closer to site center, the denser the sampling points. This naturally represents the characteristic of the 3D mass points generated from ground-based photogrammetry.

2.3. cvrDEM data structure

As mentioned earlier, though the sampling points of the cvrDEM are not evenly distributed, they are regularly distributed and can be stored in a matrix form as a traditional grid-based DEM is. We only need to store the necessary parameters and the elevation values of the sampling points. Referring to a popular ASCII DEM format, we define the data structure of the cvrDEM, which is listed in Table 2.

As shown above, the cvrDEM structure consists of header information containing a set of keywords, followed by cell values in row-major order:

(1) Header information: include the Cartesian coordinates of the site center (X_O, Y_O), the minimum angle θ_{min} and the number of rows N_θ, the minimum range r_{min} and the number of columns N_r, the radial resolution coefficient λ and the angular resolution δ_θ, and nodata_value. The nodata_value is the value in the ASCII file to be assigned to those cells whose true value is unknown. Its default value is set to be −99,999.
(2) Cell values: a matrix of the elevation values in row-major order. The number of cell values is equal to the number of rows N_θ times the number of columns N_r in the header.

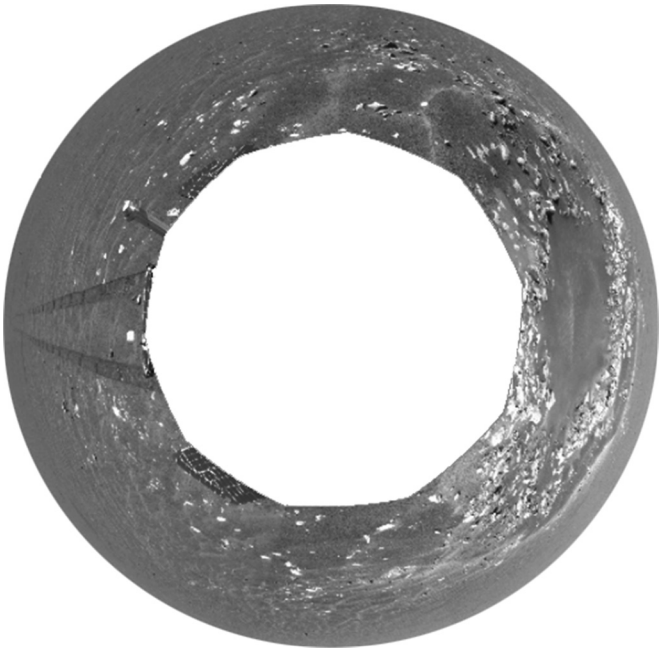

Fig. 6. Polar mosaic of the panorama.

As cvrDEM can arrange the sampling points in order, its data structure implicitly covers the topological adjacencies. In comparison with TIN, it can reduce storage size while implicitly maintaining spatial relationship. In comparison with grid-based DEM, the cvrDEM can represent terrain relief more precisely and save storage space.

3. Experimental results

3.1. Navcam images of Mars exploration rover (MER)

Navcam images acquired by the NASA MER rover Opportunity were used in this study. The image data and associated point cloud data were downloaded from the publically accessible MER Analyst's Notebook website[1] at Washington University in St. Louis.

[1] http://an.rsl.wustl.edu/mer/.

Among the numerous imaging sensors carried by Opportunity, Navcam is a pair of monochrome stereo cameras mounted on the camera bar of the rover. Navcam images have been constantly in use during mission operations for navigation and terrain mapping (Li et al., 2005). The epipolar-resampled Navcam images were used in our experiment. These images are published in PDS (Planetary Data System) format and defined as FFL files. Fig. 5 shows Opportunity rover images acquired by Navcam on Sol 85. Fig. 6 is a polar mosaic map of the images generated by our own software. The small crater in the images is Fram Crater.

Table 3
Fram Crater cvrDEM parameters.

Header information	value
Site center coordinates	(161.466, 168.911)
θ_{min} and r_{min}	0.000 and 0.869
N_θ and N_r	1571 and 740
δ_θ and λ	0.004 and 0.004
nodata_value	−99,999

Three-dimensional point cloud data derived from stereo images are defined as XYL files in the MER Analyst's Notebook. The data are stored with the index of the left image of each stereo pair and the pixel values are ground coordinates X, Y, and Z in the local site coordinate system (Di et al., 2008). The data are also published in PDS format. After all the point cloud data files for the panorama were combined and filtered, 71,843 feature points were obtained. Based on these points, 1,130,579 sampling points of the cvrDEM were generated using the parameters listed in Table 3. In this experiment, λ and δ_θ are determined in Eqs. (4) and (5) by setting n and m to be 5.

Fig. 7a shows the final cvrDEM product (up to a range of 16 m) with resolution varying from 0.004 m to 0.067 m. Fig. 7b is an enlarged view of the area outlined by a rectangle in Fig. 7a. For comparison purposes, we also produced a grid DEM that covers an area of 32 m × 32 m with a resolution of 0.030 m per

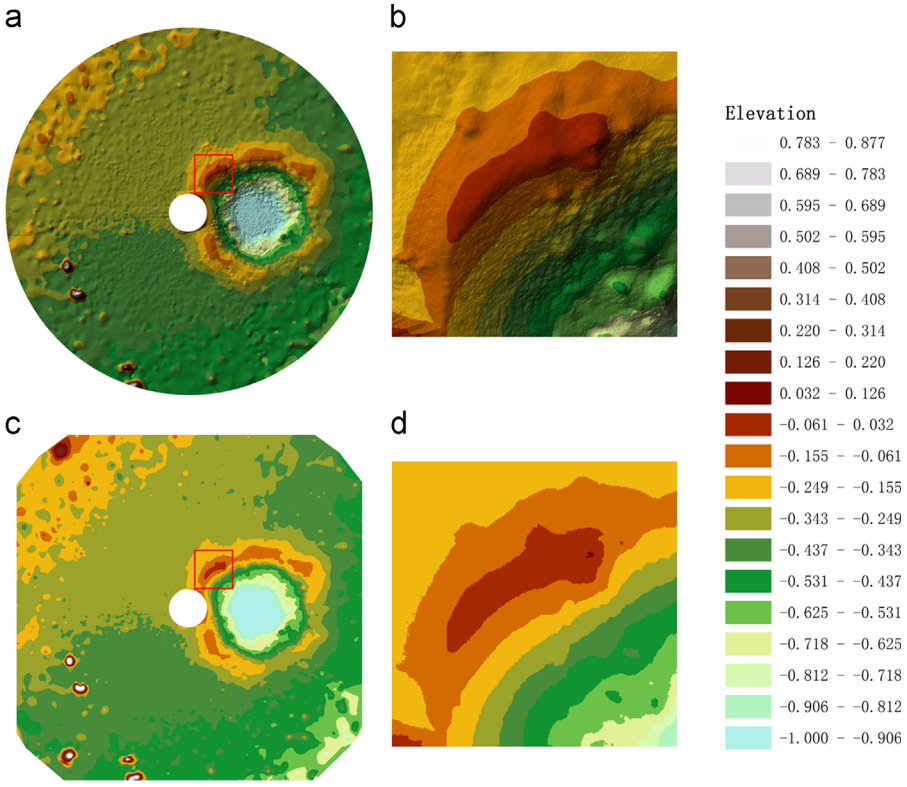

Fig. 7. (a) cvrDEM, (b) enlarged view of the area outlined by a rectangle in (a), (c) grid DEM, and (d) enlarged view of the area outlined in (c).

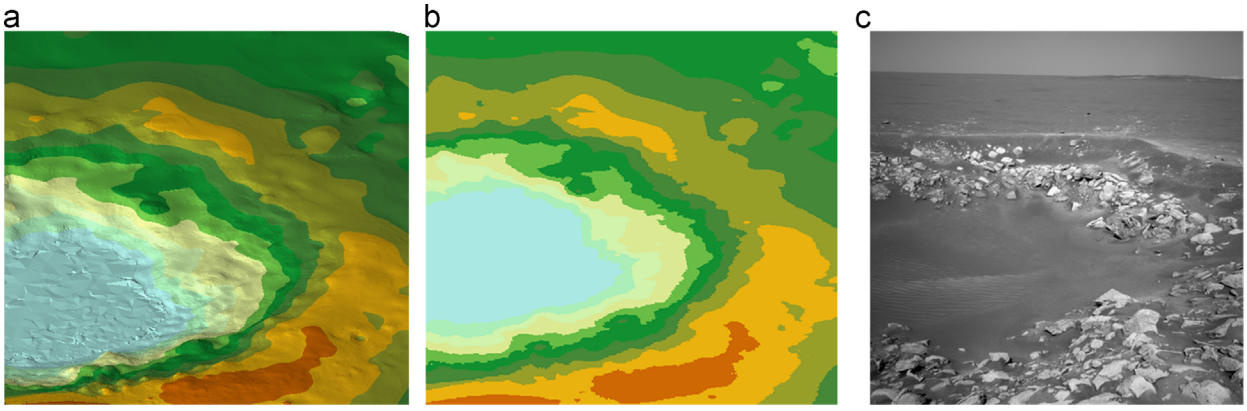

Fig. 8. (a) Perspective view of cvrDEM, (b) perspective view of grid DEM, and (c) original Navcam image.

Table 4
Comparison of file sizes of cvrDEM and grid DEMs.

	row × col	ASCII file size (M)	Resolution (m)
cvrDEM	1571 × 740	6.66	0.004–0.067
grid DEM	10,000 × 10,000	366	0.004
grid DEM	1078 × 1078	6.66	0.030

pixel (so that its file size is the same as that of the cvrDEM). Fig. 7c and d shows the corresponding grid DEM and an enlarged view. It can be clearly observed that the cvrDEM has much more terrain detail than the grid DEM, especially in the near range.

In addition, we produce local perspective views of the cvrDEM and the grid DEM and compare them with the original Navcam imagery. As illustrated in Fig. 8, it can be clearly seen that the cvrDEM can reveal more details in the near range than the grid DEM, and produces details more comparable to the original image.

The cvrDEM has a variable radial resolution from 0.004 m to 0.067 m that varies to maintain the mapping accuracy. On the other hand, a grid DEM with the same file size (similar ASCII format) has a fixed resolution of 0.030 m that is corresponding to the resolution of the cvrDEM at a range of 7.26 m. Therefore, in the grid DEM the terrain is under-sampled (losing accuracy) for ranges less than 7.26 m from the site center and over-sampled for ranges over 7.26 m (wasting storage space).

If the highest resolution of 0.004 m is adopted for the grid DEM, its file size will be 366 M, which is 55 times larger than the cvrDEM. For clear comparison, we summarized file size information for the cvrDEM and the two grid DEMs in Table 4.

It is worth noting that visualization products from the cvrDEM are different from those from a grid DEM. One simple method is to convert the cvrDEM data to TIN on-the-fly and then visualize the TIN. Since the sampling points of cvrDEM are regularly distributed, the conversion is straightforward and very fast. This is how the cvrDEM was visualized for Figs. 7 and 8.

3.2. Terrestrial laser scanning data

A data set of terrestrial laser scanning points was used to further evaluate the developed cvrDEM model. The point cloud data were downloaded from Canadian Planetary Emulation Terrain 3D Mapping Dataset[2] of the Canadian Space Agency's (CSA) Mars Emulation Terrain (MET), which is an outdoor test facility located near Montreal, Quebec, Canada. The terrain consists of scattered rocks on sand, along with some large ridges, craters, and outcrop features. Surveying of the terrain was performed using SICK LMS111-10100 laser rangefinder, which has a nominal range accuracy of 12 mm and an angular resolution of 0.25°. The point cloud data of the 43rd scan, which has 1,134,633 feature points and approximately covers an area of 37 m × 37 m, was used in our experiment. Fig. 9 shows the point cloud of this data set after sampling down to 50,000 points for clearer visualization.

The parameters for generating cvrDEM from this terrestrial laser scanning data are listed in Table 5. As a result, 1,159,398 sampling points of the cvrDEM were generated based on the feature points. Fig. 10a shows the final cvrDEM product. Fig. 10b is an enlarged view of the area outlined by a rectangle in Fig. 10a. For comparison purpose, a grid DEM was also produced that covers an area of 37 m × 37 m with a resolution of 0.035 m per pixel so that the DEM has the same number of cvrDEM points (resulting in the same file size). Fig. 10c and d shows the corresponding grid DEM and an enlarged view. According to the enlarged view ridges and rocks are clearly shown in cvrDEM, while in the grid DEM these features are almost missing.

[2] http://asrl.utias.utoronto.ca/datasets/3dmap/box_met.html.

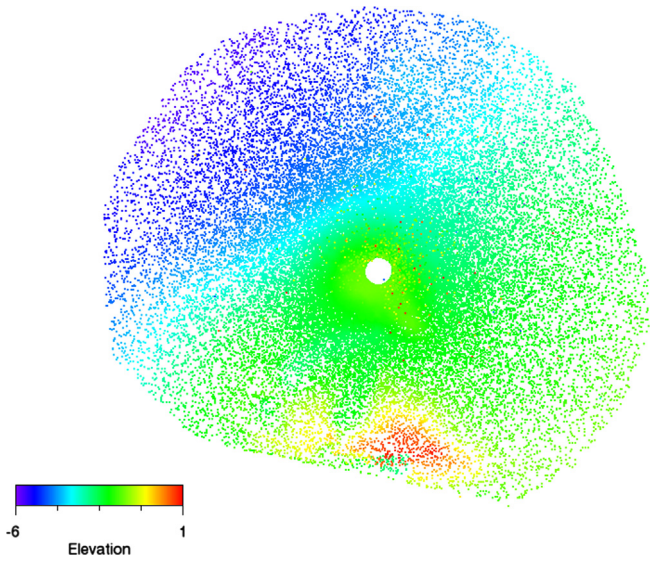

Fig. 9. Point cloud of a terrestrial laser scanning data (after sampling for clear visualization).

Table 5
cvrDEM parameters for the terrestrial laser scanning data.

Header information	value
Site center coordinates	(0, 0)
θ_{min} and r_{min}	0.000 and 1.000
N_θ and N_r	1571 and 732
δ_θ and λ	0.004 and 0.004
nodata_value	−99,999

Results of the above experiments show that the cvrDEM is superior to the traditional grid DEM in representing the digital terrain produced through ground-based photogrammetry and terrestrial laser scanner. It can maintain the mapping accuracy and achieve storage efficiency, offering the best overall performance.

4. Conclusions

This research developed a continuative variable-resolution DEM model for the representation of 3D terrain generated by photogrammetric processing of ground-based imagery. From theoretical analysis and experimental results, the following conclusions can be drawn:

(1) cvrDEM is very valuable for photogrammetric processing of ground-based imagery because it is capable of maintaining the different mapping accuracies at different ranges with variable resolutions while reducing data storage space significantly.
(2) In cvrDEM construction, the radial resolution changes gradually according to the range-dependent mapping accuracy while the angular resolution remains constant. As a result, denser points are sampled in the near range while sparser points are sampled in the far range, representing well the characteristics of the mass 3D points generated from ground-based stereo imagery. With the same file size, the cvrDEM can preserve much more terrain detail than a traditional grid DEM.
(3) Since the sampling points of cvrDEM are unevenly but regularly distributed, they can be efficiently stored and accessed

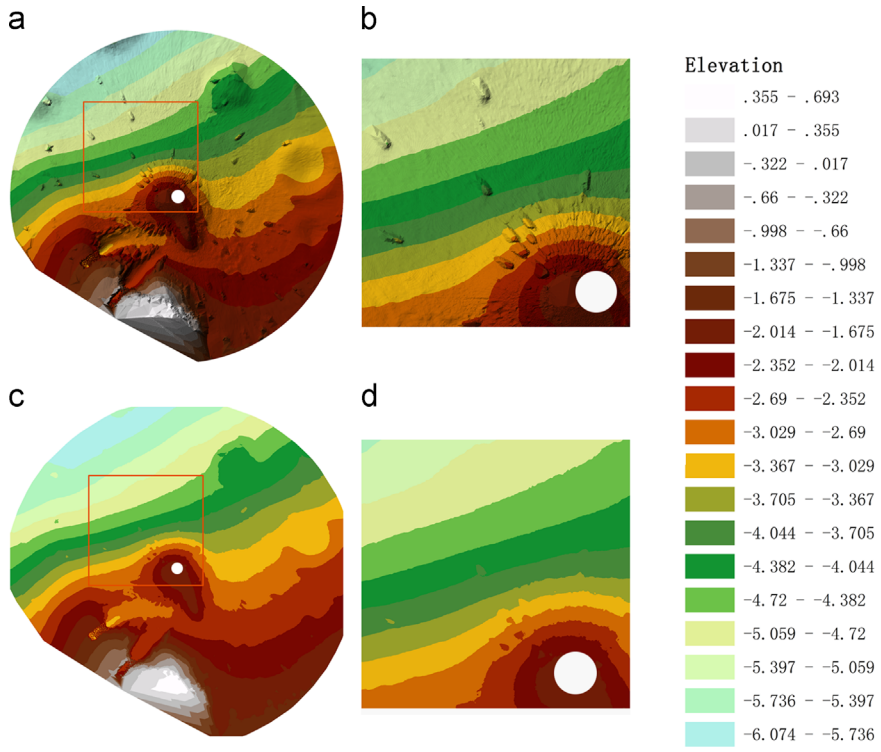

Fig. 10. DEMs generated from terrestrial laser data: (a) cvrDEM, (b) enlarged view of the area outlined by a rectangle in (a), (c) grid DEM, and (d) enlarged view of the area outlined in (c).

in a cvrDEM database structure that is similar to that of a grid DEM.

In the near future, we will develop more terrain products (such as slope maps and aspect maps) and spatial analysis algorithms based on cvrDEM. We will also validate the performance of cvrDEM using more data generated from photogrammetric processing of ground-based imagery and terrestrial laser scanning data. Investigation of other possible variable resolution digital elevation models and comparison with the cvrDEM will also be open topic for future research.

Acknowledgments

The work described in this paper was supported by the National Basic Research Program of China (Project no. 2013CB733202), National Natural Science Foundation of China (Project nos. 41171355 and 41201480) and the Open Research Foundation of Science and Technology on Aerospace Flight Dynamics Laboratory (Grant no. 2012afdl039). The image data used in the experiment were downloaded from MER Analyst's Notebook website (http://an.rsl.wustl.edu/mer/) at Washington University in St. Louis. The terrestrial laser scanning data were downloaded from Autonomous Space Robotics Lab website (http://asrl.utias.utoronto.ca/datasets/3dmap/box_met.html) at the University of Toronto Institute.

References

Alexander, D.A., Deen, R.G., Andres, P.M., Zamani, P., Mortensen, H.B., Chen, A.C., Cayanan, M.K., Hall, J.R., Klochko, V.S., Pariser, O., 2006. Processing of Mars Exploration Rover imagery for science and operations planning. J. Geophys. Res.-Planets 111 (E2), E02S02.

Bertolotto, M., Floriani, L.D., Puppo, E., 1994. Hierarchical hypersurface modeling. In: Proceedings of the International Workshop on Advanced Information Systems: Geographic Information Systems, pp. 88–97.

De Floriani, L., Marzano, P., Puppo, E., 1996. Multiresolution models for topographic surface description. Visual Comput. 12 (7), 317–345.

Di, K., Li, R., 2007. Topographic mapping capability analysis of Mars Exploration Rover 2003 mission imagery. In: Proceedings of the 5th International Symposium on Mobile Mapping Technology, Padua, Italy, 7p.

Di, K., Xu, F., Wang, J., Agarwal, S., Brodyagina, E., Li, R., Matthies, L., 2008. Photogrammetric processing of rover imagery of the 2003 Mars Exploration Rover mission. ISPRS J. Photogrammetry Remote Sensing 63 (2), 181–201.

Evans, W., Kirkpatrick, D., Townsend, G., 2001. Right-triangulated irregular networks. Algorithmica 30 (2), 264–286.

Fredrik, L., Jungert, E., 2000. Dual aspects of a multi-resolution grid-based terrain data model with supplementary irregular data points. In: Proceedings of the Third International Conference on Information Fusion, Paris, France, pp. 403–410.

Li, R., Squyres, S.W., Arvidson, R.E., Archinal, B.A., Bell, J., Cheng, Y., Crumpler, L., Marais, D.J.D., Di, K., Ely, T.A., Golombek, M., Graat, E., Grant, J., Guinn, J., Johnson, A., Greeley, R., Kirk, R.L., Maimone, M., Matthies, L.H., Malin, M., Parker, T., Sims, M., Soderblom, L.A., Thompson, S., Wang, J., Whelley, P., Xu, F.L., 2005. Initial results of rover localization and topographic mapping for the 2003 Mars Exploration Rover mission. Photogrammetric Eng. Remote Sensing 71 (10), 1129–1142.

Li, Z., Zhu, Q., Gold, C., 2004. Digital Terrain Modelling: Principles and Methodology. CRC Press p. 323.

Mahdi, A., Wynne, C., Cooper, E., Roy, L., 1998. Representation of 3-D elevation in terrain databases using hierarchical triangulated irregular networks: a comparative analysis. Int. J. Geogr. Inf. Sci. 12 (8), 853–873.

Maki, J.N., Bell III, J.F., Herkenhoff, K.E., Squyres, S.W., Kiely, A., Klimesh, M., Schwochert, M., Litwin, T., Willson, R., Johnson, A., Maimone, M., Baumgartner, E., Collins, A., Wadsworth, M., Elliot, S.T., Dingizian, A., Brown, D., Hagerott, E.C., Scherr, L., Deen, R., Alexander, D., Lorre, J., 2003. Mars exploration rover engineering cameras. J. Geophys. Res.-Planets 108 (E12), 8071.

Masuda, T., 2009. Log-polar height maps for multiple range image registration. Comput. Vision Image Understanding 113 (11), 1158–1169.

Maune, D.F., 2007. Digital Elevation Model Technologies and Applications: The DEM Users Manual. Am. Soc. Photogrammetry Remote Sensing, 655.

Moore, I.D., Grayson, R., Ladson, A., 2006. Digital terrain modelling: A review of hydrological, geomorphological, and biological applications. Hydrol. Processes 5 (1), 3–30.

Oliveira, A., Oliveira, J.F., Pereira, J.M., de Araújo, B.R., Boavida, J, 2012. 3D modelling of laser scanned and photogrammetric data for digital documentation: The Mosteiro da Batalha case study. J. Real-Time Image Process., 1–16, http://dx.doi.org/10.1007/s11554-012-0242-0.

Onkarappa, N., Sappa, A.D., 2013. A novel space variant image representation. J. Math. Imaging Vision 47 (1), 48–59.

Pajarola, R., 2002. Overview of Quadtree-Based Terrain Triangulation and Visualization. Department of Information & Computer Science, University of California, Irvine. (16pp).

Pajarola, R., Gobbetti, E., 2007. Survey of semi-regular multiresolution models for interactive terrain rendering. Visual Comput. 23 (8), 583–605.
Slama, C.C., Theurer, C., Henriksen, S.W., 1980. Manual of Photogrammetry. American Society of Photogrammetry, Falls Church, VA. (1056pp).
Suárez, J.P., Plaza, A., 2009. Four-triangles adaptive algorithms for RTIN terrain meshes. Math. Comput. Model. 49 (5), 1012–1020.
Traver, V.J., Bernardino, A., 2010. A review of log-polar imaging for visual perception in robotics. Rob. Auton. Syst. 58 (4), 378–398.
Wang, Z, 1990. Principles of Photogrammetry with Remote Sensing. Press of Wuhan Technical University of Surveying and Mapping, Wuhan p. 575.
Wilson, J.P., Gallant, J.C., 2000. Terrain Analysis: Principles and Applications. Wiley, New York p. 15.
Wolberg, G., Zokai, S., 2000. Robust image registration using log-polar transform. In: Proceedings of the IEEE International Conference on Image Processing, Vancouver, Canada, pp. 493–496.
Xie, X., Xu, W., Zhu, Q., Zhang, Y., Du, Z., 2013. Integration method of TINs and Grids for multi-resolution surface modeling. Geo-spatial Inf. Sci. 16 (1), 61–68.
Zhao, W., Tao, T., Gong, H., Duan, F., Mo, Y., 2006. Dynamic data retrieval and distance decay of triangulated irregular network(TIN) in three dimensional visualizations. Geogr. Inf. Sci.: J. Assoc. Chin. Prof. Geogr. Inf. Syst. 12 (1), 21–26.
Zarrabeitia, L.A., Mederos, V.H., 2013. Multiresolution terrain modeling using level curve information. J. Comput. Appl. Math. 240 (1), 87–98.
Zhang, L., Yang, C., Liu, D., Ren, Y., Rui, X., 2005. A web-mapping system for real-time visualization of the global terrain. Comput. Geosci. 31 (3), 343–352.